Journal of Physics: Conference Series

PAPER • **OPEN ACCESS**

The crack surface morphology investigation of S355J2 steel after bending-torsion fatigue

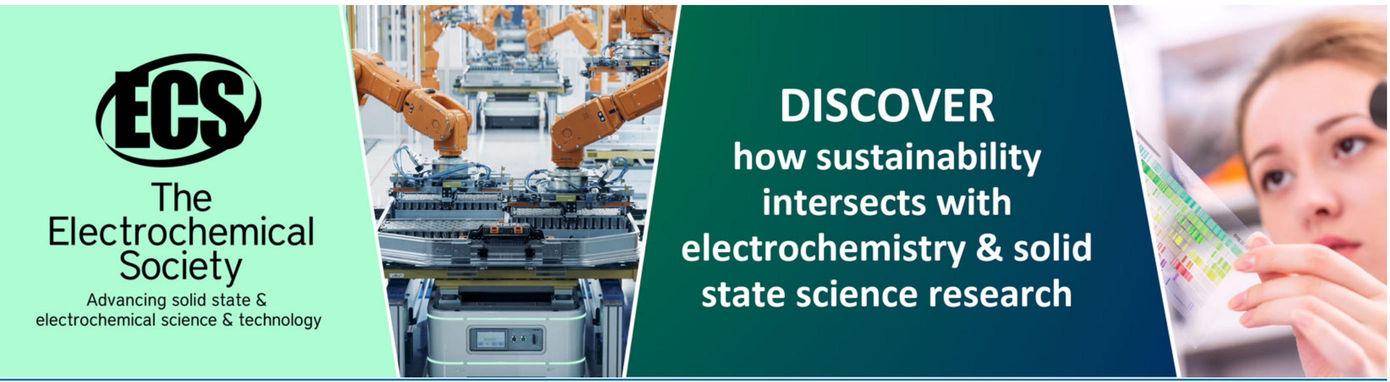

The crack surface morphology investigation of S355J2 steel after bending-torsion fatigue

W Macek[1], Z Marciniak[2], R Branco[3], M Szala[4] and A Rehmus-Forc[5]

[1] University of Occupational Safety Management in Katowice, ul. Bankowa 8, 40-007 Katowice, Poland
[2] Opole University of Technology, Faculty of Mechanical Engineering, Department of Mechanics and Machine Design, 5 Mikołajczyka Street, 45-271 Opole, Poland
[3] University of Coimbra, CEMMPRE, Department of Mechanical Engineering, Rua Luís Reis Santos, Pinhal de Marrocos, 3030-788 Coimbra, Portugal
[4] Lublin University of Technology, Faculty of Mechanical Engineering, Department of Materials Engineering, 36 Nadbystrzycka Street, 20-618 Lublin, Poland
[5] State University of Applied Sciences in Elbląg, ul. Wojska Polskiego 1, 82-300 Elbląg, Poland

wojciech.macek@yahoo.com

Abstract. The paper describes the analysis of crack surface morphology of S355J2 steel specimens after bending-torsion fatigue. These experimental investigations of the surface topography were carried out using the focus variation microscope, an optical 3D measurement device. Selected results of measured fracture surfaces for S355J2 steel were analysed according to the surface texture ISO 25178 standard. Differences in roughness values for different loadings were demonstrated. For profile Rx and areal Sx parameters, characteristic relationships of fracture zones have been demonstrated. It has been shown that roughness profile Ra for the rupture area is higher than for the propagation area, as well as increases after both the LCF and HCF tests and increases with the torsional loading level. However, Sa in the propagation area increases and the rupture area decreases.

1. Introduction

Engineering materials are sharpened in specific geometries to withstand the loads subjected to the components and structures. Among many grades of engineering metallic materials, steel still seems the most popular material applied for many types of structures [1–3]. The machine parts made of steel are traditionally formed or strengthened in casting, plastic forming, machining, welding, or heat treatment processes [4–6]. All mentioned processes affect the steel mechanical and functional properties and usually strongly influence the fatigue properties of a final structure. The selection of the manufacturing process has also a tremendous influence on surface quality and consequently, fatigue behaviour. It is known from the literature that fatigue testing is a time-consuming process [7–10]. Parallel to the tests, new calculation models are being developed for the determination of fatigue life and behaviour of structural materials, especially for multiaxial loadings, such as tension-torsion and bending-torsion [11–17]. Wide development in finite element method (FEM) modelling can be observed [18–23]. All these research and computational methods are supplemented with material tests at various scales [24–27] to give a possible broad spectrum of information on the material's behaviour and properties.

Fracture surface topography is one of the basic macroscopic investigations aimed at determining the cause of the damage [26, 28–33]. It allows determining what kind of loading (static or fatigue) the material was subjected to. Several typical macroscopic patterns of fatigue damage can be distinguished. Among them, there are functions of type and magnitude of loading. The surface analysis reveals the localisation of initiation sites and crack paths, as well as identifies the areas for further microscopic examination [34–36]. Fracture mechanics tests are usually concentrated on crack growth under uniaxial and/or multiaxial loadings [37–41]. Some articles focus on crack growth, while other scientists carried out a quantitative analysis of fracture surface [42–45]. The study on the relationship between fracture toughness and fracture surface fractal dimension began in the 1980s [46–49]. Since then, the quantitative approach to the morphology has led to many interesting studies on the interconnection with loading or ambient environment [26, 50–52].

The topography of fracture surfaces, especially in bending and torsion fatigue, was investigated and published in [53–56]. Researchers demonstrated, inter alia, the influence of torsion loading constituent on the surface form. Until now, several publications by Macek and others have been published describing the properties of entire fracture surface topography after bending-torsion fatigue [57–60]. Therefore, this research is a continuation of the previously published papers and proceeds the state of art in the field of fracture analysis.

Multiaxial loading is a critical issue in mechanical design that requires tuned engineering approaches. Therefore, firstly, in the study of the multiaxial fatigue behaviour of S355J2 steel, and then using advanced metrology, we quantified the state of surface topography. The aim of this paper is to study the relationship between the arithmetical mean deviation of the roughness profile, Ra, and the arithmetical mean height, Sa, of fracture surfaces and the loading types [61, 62].

2. Materials and methods

2.1. Steel S355J2 fatigue test

Fatigue tests on hourglass specimens made of S355J2 steel were performed on an MZGS test stand [63–65]. An example of the broken specimen of steel S355J2 subjected to non-proportional bending with torsion is shown in Figure 1. The material was characterised by the chemical composition and mechanical properties shown in Tables 1 and 2, respectively. The fracture surface analysis was conducted on steel specimens subjected to fatigue random bending and combination bending with torsion loadings. In order to distinguish in a simple way, the type of loading the stress ratio ($\lambda = \tau_{max}/\sigma_{max}$) was employed.

Figure 1. Damaged specimen after bending-torsion fatigue.

Table 1. Chemical composition of steel S355J2 in wt.% [66].

C	Mn	Si	P	S	Cr	Ni	Cu	Fe
0.21	1.46	0.42	0.019	0.046	0.09	0.04	0.17	Balance

Table 2. The mechanical properties of the S355J2 steel [66].

σ_y, MPa	σ_U, MPa	A_{10}, %	RA, %	E, GPa	ν
357	535	21	50	210	0.30

2.2. Fracture surface investigation

In this work, the roughness of the newly created fracture plane and the effect of load combinations on surface formation were analysed. Profile (linear) and surface roughness indicators were used to qualify the surface [67–69]. The analysis was performed using the focus variation microscope Alicona Infinite Focus, an optical 3D measurement device, which allows the acquisition of data sets with a large depth of focus [70–72]. The measurement device was equipped with a motorised nosepiece using a set of five dedicated microscopic objective lenses with 2.5×, 5×, 10×, 20×, 50×, and 100× magnification. For profiles measurement, the total area of the fatigue crack was investigated at the objective magnification of 10×. To perform total area scanning, the Imagefield function was used; for initiation and propagation areas check, the selected specimens' zones were analysed with the magnification of 100×.

2.2.1. Propagation and rupture profile parameters

Roughness measurements were carried out in two areas of the fracture surface, first in the propagation area and second in the rupture area (Figure 2), representative 2 mm measurement profile length was chosen for all examined specimens. Due to the strong influence of filter waviness, L_c, on roughness measurements a constant value L_c = 250 μm was used. Profiles in the rupture area are so conventionally named, as we can see in the case for Figure 2a, the rupture starts a little higher.

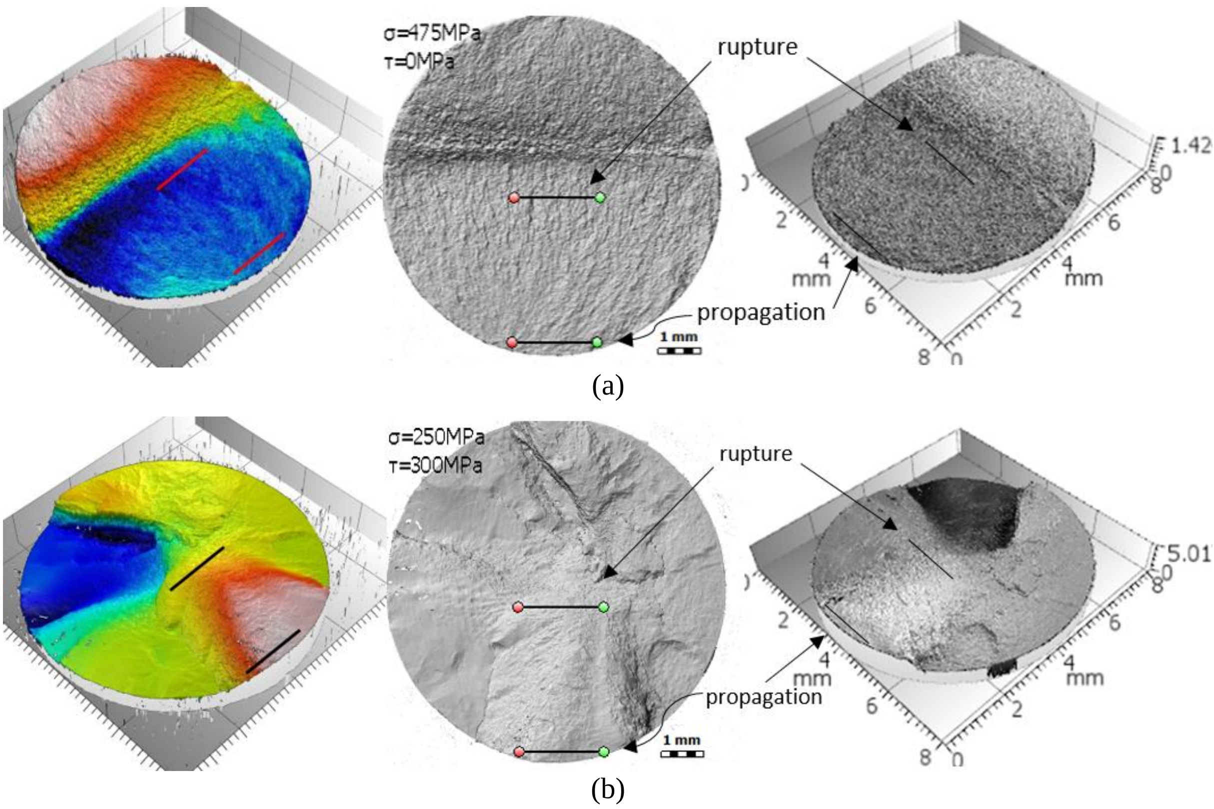

Figure 2. Steel S355J2 specimen subjected to combined bending-torsion loading with marked crack propagation and rupture roughness profiles, for exemplary specimens' loadings a) σ_{max} = 475 MPa, τ_{max} = 0 MPa, b) σ_{max} = 250 MPa, τ_{max} = 300 MPa.

2.2.2. Areal parameters for selected propagation and rupture areas

The measurements of propagation and rupture zones were made with a magnification of 100× for selected samples. Figure 3 shows the fracture planes with selected zones for areal parameters Sx measurement. On the left-side, pictures present the propagation areas; on the right-side, we can see the rupture areas.

Observing the surfaces, we can note the difference in granularity and roughness of the fracture plane. For samples subject to uniaxial loading, the surface structure is fine-grained both in the propagation zone and in the rupture zone. However, for samples subjected to a combination of bending loads and torsion, there are significant differences between both zones. In the propagation zone, larger differences in surface grain are visible, as well as their directionality, which is manifested by elongated grains. Whereas the rupture zone, this directivity disappears.

a)
b)
c)
d)
e)

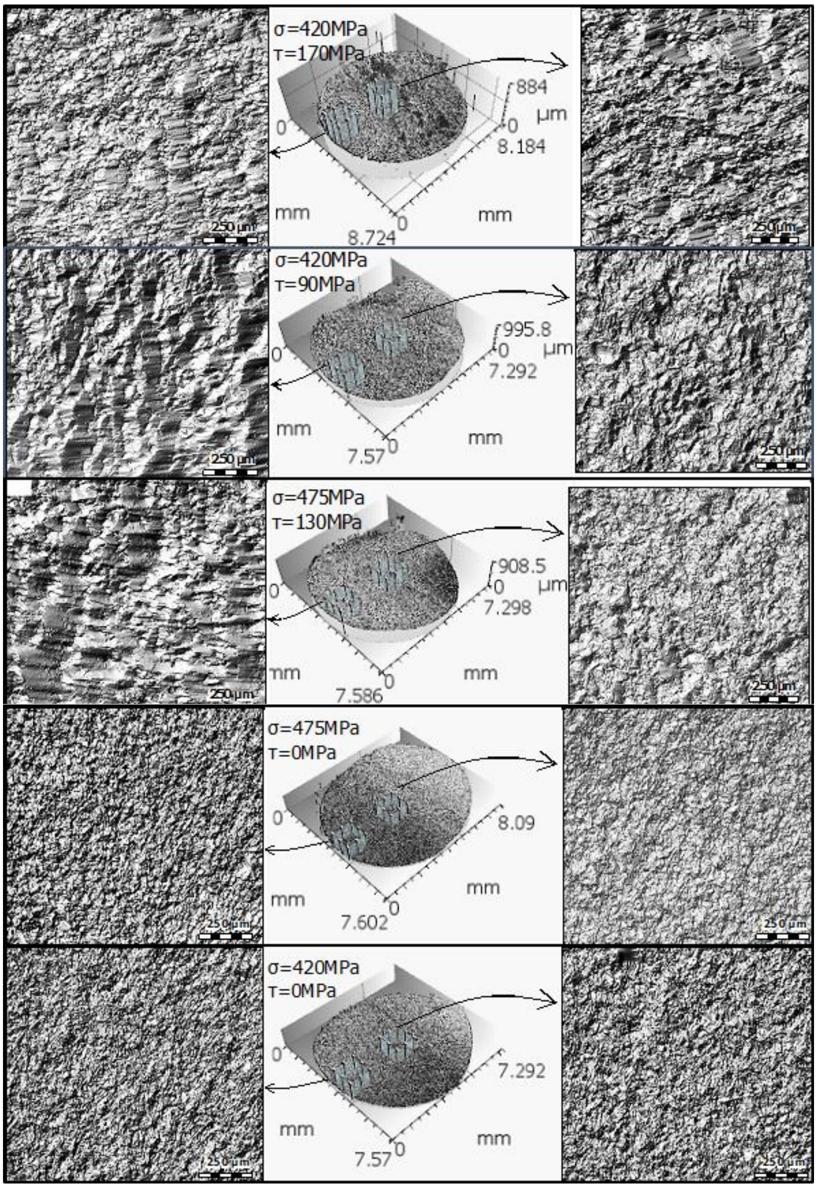

Figure 3. Selected steel S355J2 specimen with exposed propagation and rupture areas for (a)-(c) different combinations of bending with torsion loadings, d) and e) bending.

3. Results and discussion

Profile Rx and areal Sx parameters, roughness profile, Ra, and also arithmetical mean height, Sa, respectively, were selected for further analyses. These parameters have the best fit to the characteristic relationships of fracture zones. Ra (Eq. (1)) averages all peaks and valleys of the roughness profile and then neutralises the few outlying points so that the extreme points have no significant impact on the final results. As far as the Sa is concerned, as expressed in Eq. (2), it represents the mean height of the surface, according to the ISO 25178 standard.

$$Ra = \frac{1}{lr}\int_0^{lr} |z(x)|dx \tag{1}$$

$$Sa = \frac{1}{A}\int_A |z(x,y)|dxdy \tag{2}$$

3.1. Profile

Exemplary results for representative profiles are shown in Figure 4. As we can see, the tendency of the roughness parameters Ra for the representative rupture area is higher than that for the representative propagation area.

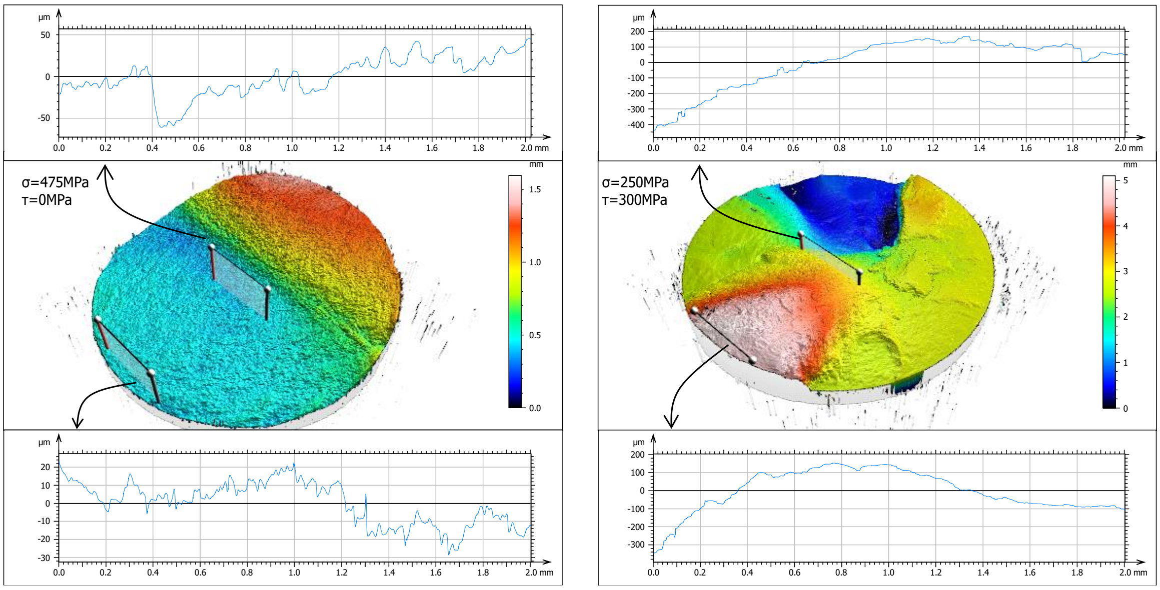

(a) (b)

Figure 4. Isometric view and profile diagrams of steel S355J2 specimen subjected to combined bending-torsion loading, for the propagation area and the rupture area: a) λ=0, and b) λ=1.2.

Figure 5 shows the relation of Ra parameter to the loading ratio, λ, in the low-cycle fatigue (LCF) and the high cycle fatigue (HCF) regimes. The obtained results show an increase in the roughness of Ra parameter as the share of shear stress τ_{max} increases. This trend is preserved both in the propagation area as well as in the rapture area. When comparing the roughness parameters of both areas, 2.43 times increase in the arithmetical mean value of roughness is observed, with the minimum value of 1.30 times and the maximum one 4.44 times. Considering the LCF and HCF tests, the arithmetical mean value of Ra amounted respectively 2.43 times and 2.44 times. The range of increase for LCF and HCF tests was respectively from 1.30 to 4.44 times and from 1.73 to 3.34 times. Despite the apparent differences in the Ra roughness values for both areas, other parameters or factors that can better describe the cracked surface and classify the load should be distinguished. This shall enable the engineer to introduce a new useful tool concerning damage analysis.

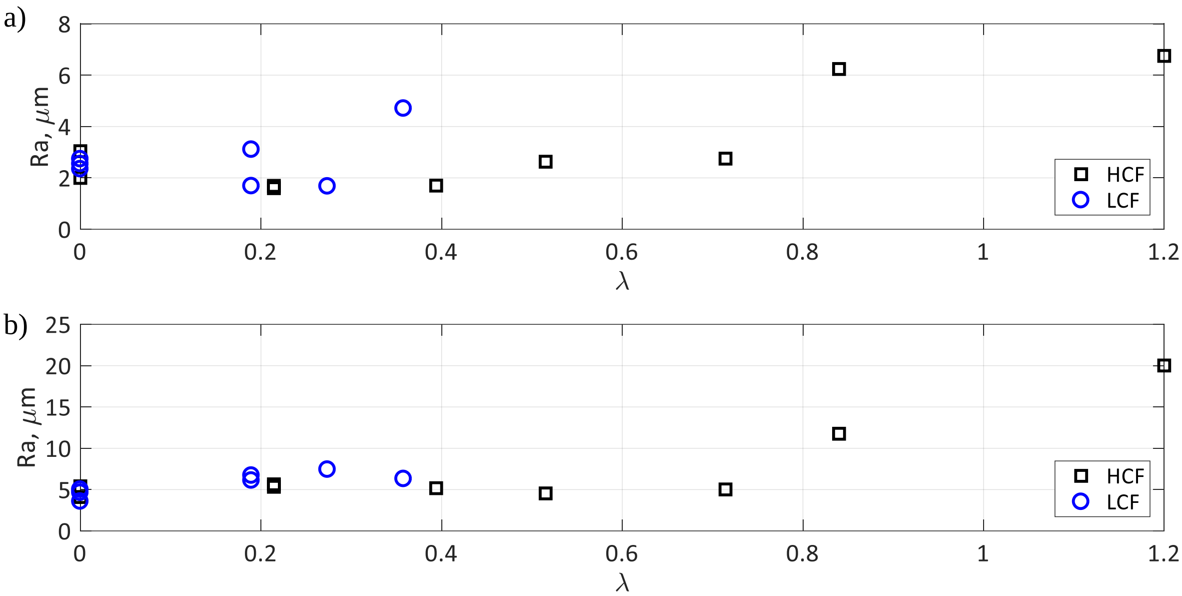

Figure 5. Relation of Ra parameter to the loading ratio λ for high cycle fatigue (HCF) and low cycle fatigue (LCF) on a) the propagation area, b) the rupture.

3.2. Areal parameter results

Figure 6 shows examples of measured propagation and rupture areas.

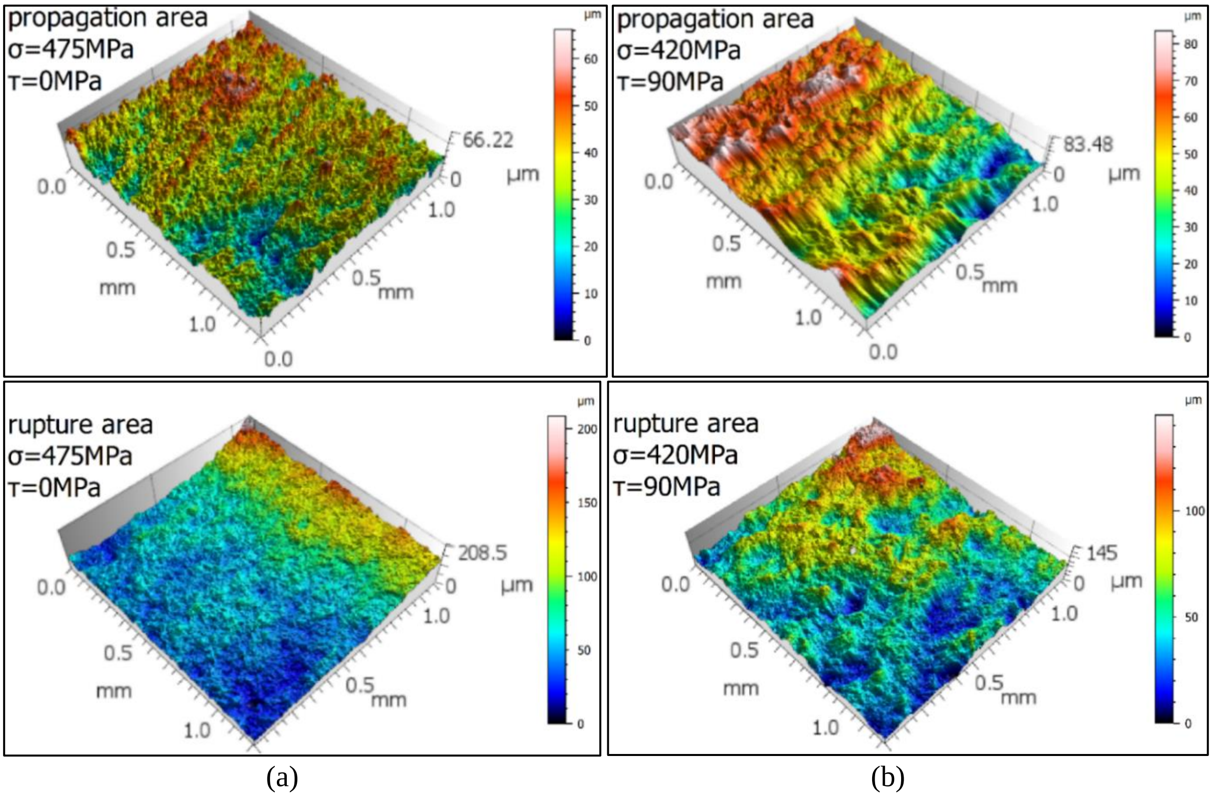

Figure 6. Isometric view of steel S355J2 specimen for the propagation area and the rupture area for a) λ=0 bending, and b) λ=0.214 bending with torsion.

Figure 7 plots the surface parameter (Sa) against the bending moment to the torsion moment ratio (λ). The figure clearly shows that arithmetical mean height (Sa) takes higher values for the rupture area. Differences between areas decrease as the loading ratio (λ) increases. The largest difference occurs for the loading ratio λ=0 and is 4.07 times, while the smallest for the loading ratio λ=0.405 and is 1.35 times. These differences are related to the fact that the parameter arithmetical mean height (Sa) decreases with the loading ratio (λ) for the propagation area and vice-versa for the rupture area.

Further analysis of the topography of fracture surface ought to be conducted in order to find out the best parameter characterising the fatigue loading history and fracture of materials, after destruction. Continued results about fracture surface characterization will be presented in forthcoming publications.

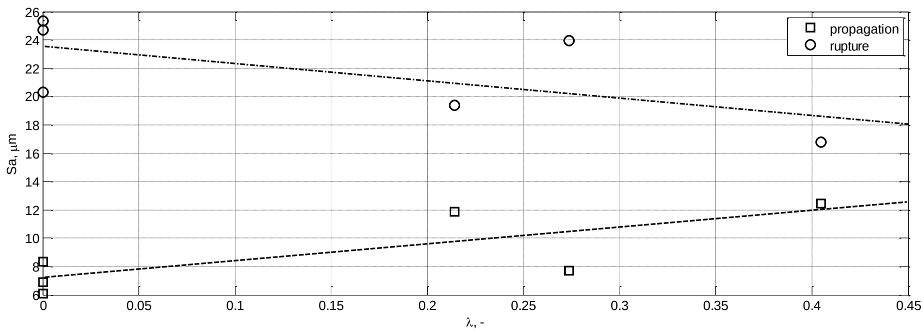

Figure 7. Relation of Sa parameter to the loading ratio λ for the propagation and the rupture area.

4. Summary

Based on the measurements and observations obtained, it can be stated that:
- arithmetical mean deviation of the roughness profile Ra, for the rupture area, is 2.43 times higher, in arithmetical mean value, than for the propagation area.
- the Ra parameter, for rupture and propagation area, increases for the same value about 2.43, in arithmetical mean, after both the LCF and HCF tests.
- differences of Sa values between the propagation and the rupture areas are higher for the loading ratio λ=0 and is 4.07 times, while the smallest for the loading ratio λ=0.405 and is 1.35 times.
- the increase in the torsional loading level increases the roughness Ra of the fracture surface for both, propagation and rupture areas. For Sa, in the propagation area, it increases; and, in the rupture area, it decreases.

References

1. S. Hashmi, *Comprehensive Materials Finishing* (Elsevier, Kidlington, Oxford, UK, 2017)
2. A. K. Rakhit, *Heat Treatment of Gears: A Practical Guide for Engineers* (ASM International, Materials Park, OH, 2000)
3. M. Kowal, M. Łagoda, *Roads and Bridges - Drogi i Mosty*. **16**, 85–99 (2017)
4. B. L. Ferguson, Z. Li, A. M. Freborg, *Computational Materials Science*. **34**, 274–281 (2005)
5. M. Szala, G. Winiarski, Ł. Wójcik, T. Bulzak, *Materials*. **13**, 2022 (2020)
6. A. Świerczyńska, M. Landowski, *Materials*. **13**, 3888 (2020)
7. R. Branco, P. A. Prates, J. D. Costa, L. P. Borrego, F. Berto, A. Kotousov, F. V. Antunes, *International Journal of Fatigue* (2019), doi:10.1016/J.IJFATIGUE.2019.02.005
8. M. Kowal, M. Szala, *Engineering Failure Analysis*. **110**, 104447 (2020)
9. G. Lesiuk, B. Rymsza, J. Rabiega, J. A. F. O. Correia, A. M. P. De Jesus, R. Calcada, *Engineering Failure Analysis*. **96**, 409–425 (2019)
10. M. P. Valles González, M. García-Martínez, A. Pastor Muro, *Engineering Failure Analysis*. **98**, 150–155 (2019)

11. M. Fonte, V. Infante, L. Reis, M. Freitas, *Engineering Failure Analysis* (2017), doi:10.1016/j.engfailanal.2017.06.010
12. R. Branco, F. V. Antunes, J. D. Costa, F. P. Yang, Z. B. Kuang, *Engineering Fracture Mechanics* (2012), doi:10.1016/j.engfracmech.2012.07.009
13. L. Susmel, N. Petrone, *European Structural Integrity Society*. **31**, 83–104 (2003)
14. A. Karolczuk, *Engineering Fracture Mechanics*. **73**, 1629–1652 (2006)
15. J. Jamali, M. J. Mahmoodi, M. K. Hassanzadeh-Aghdam, J. T. Wood, *Composites Part B: Engineering*. **176**, 107316 (2019)
16. A. Niesłony, M. Böhm, R. Owsiński, *International Journal of Fatigue*. **135**, 105519 (2020)
17. M. de Freitas, L. Reis, M. da Fonte, B. Li, *Engineering Fracture Mechanics*. **78**, 826–835 (2011)
18. D. Krzyzak, T. Łagoda, *International Journal of Fatigue* (2014), doi:10.1016/j.ijfatigue.2013.12.004
19. K. Falkowicz, H. Dębski, *Adv. Sci. Technol. Res. J.* **11**, 186–193 (2017)
20. L. Witek, P. Zelek, *Engineering Failure Analysis*. **97**, 374–382 (2019)
21. F. Berto, G. Fortese, C. Ronchei, D. Scorza, S. Vantadori, *Engineering Fracture Mechanics*. **174**, 44–53 (2017)
22. B. Stępak, P. Dzienny, V. Franke, P. Kunicki, T. Gotszalk, A. Antończak, *Applied Surface Science* (2018), doi:10.1016/j.apsusc.2017.12.016
23. K. Falkowicz, H. Debski, *Composite Structures*. **252**, 112701 (2020)
24. M. B. Djukic, V. Sijacki Zeravcic, G. M. Bakic, A. Sedmak, B. Rajicic, *Engineering Failure Analysis* (2015), doi:10.1016/j.engfailanal.2015.05.017
25. K. Rodak, A. Brzezińska, R. Molak, *Materials Science and Engineering A*. **724**, 112–120 (2018)
26. M. B. Djukic, G. M. Bakic, V. Sijacki Zeravcic, A. Sedmak, B. Rajicic, *Engineering Fracture Mechanics*. **216**, 106528 (2019)
27. A. Kubit, T. Trzepiecinski, W. Bochnowski, M. Drabczyk, K. Faes, *Archives of Civil and Mechanical Engineering*. **19**, 1419–1430 (2019)
28. R. Branco, F. V. Antunes, J. D. Costa, *Engineering Fracture Mechanics*. **141**, 170–195 (2015)
29. I. Miletić, A. Ilić, R. R. Nikolić, R. Ulewicz, L. Ivanović, N. Sczygiol, *Materials* (2020), doi:10.3390/ma13061301
30. M. Szala, K. Beer-Lech, M. Walczak, *Engineering Failure Analysis* (2017), doi:10.1016/j.engfailanal.2017.02.014
31. S. Sahu, P. C. Yadav, S. Shekhar, *Metallography, Microstructure, and Analysis* (2017), doi:10.1007/s13632-017-0396-z
32. Y. Cao, Y. Zhen, M. Song, H. Yi, F. Li, X. Li, *International Journal of Mechanical Sciences*. **179**, 105627 (2020)
33. D. Martelo, D. Sampath, A. Monici, R. Morana, R. Akid, *Engineering Fracture Mechanics*. **221**, 106678 (2019)
34. H. Lauschmann, K. Tesař, K. Jiroušková, *Procedia Structural Integrity*. **23**, 107–112 (2019)
35. M. Niemczewska-Wójcik, *Measurement*. **96**, 8–17 (2017)
36. G. V. K. Sai Srikanth, Z. Liu, M. J. Tan, *International Journal of Fatigue*. **130**, 105277 (2020)
37. R. Branco, P. A. Prates, J. D. Costa, L. P. Borrego, F. Berto, A. Kotousov, F. V. Antunes, *International Journal of Fatigue*. **124**, 89–98 (2019)
38. W. Macek, T. Łagoda, N. Mucha, *Fatigue and Fracture of Engineering Materials and Structures* (2017), doi:10.1111/ffe.12677
39. W. Macek, N. Mucha, *Mechanics and Mechanical Engineering*. **21**, 935–951 (2017)
40. T. Łagoda, G. Robak, J. Słowik, *Materials and Design* (2013), doi:10.1016/j.matdes.2013.04.087
41. D. Skibicki, Ł. Pejkowski, *International Journal of Fatigue* (2017), doi:10.1016/j.ijfatigue.2017.04.011
42. K. Slámečka, J. Pokluda, M. Kianicová, S. Major, I. Dvořák, *International Journal of Fatigue*. **32** (2010), doi:10.1016/j.ijfatigue.2009.07.009
43. T. Kobayashi, D. A. Shockey, *Engineering Fracture Mechanics*. **77**, 2370–2384 (2010)

44. F. V. Antunes, A. Ramalho, J. M. Ferreira, *International Journal of Fatigue* (2000), doi:10.1016/S0142-1123(00)00048-7
45. M. Meischel, S. E. Stanzl-Tschegg, A. Arcari, N. Iyyer, N. Phan, *Procedia Structural Integrity*. **2**, 1077–1084 (2016)
46. B. B. Mandelbrot, D. E. Passoja, A. J. Paullay, *Nature* (1984), doi:10.1038/308721a0
47. A. Carpinteri, A. Spagnoli, S. Vantadori, *Engineering Fracture Mechanics*. **77**, 974–984 (2010)
48. P. Kotowski, *International Journal of Fracture* (2006), doi:10.1007/s10704-006-8264-x
49. S. Morel, E. Bouchaud, J. Schmittbuhl, G. Valentin, *International Journal of Fracture* (2002), doi:10.1023/A:1015727911242
50. J. J. Mecholsky, *Dental Materials* (1995), doi:10.1016/0109-5641(95)80045-X
51. D. Sampath, R. Akid, R. Morana, *Engineering Fracture Mechanics*. **191**, 324–343 (2018)
52. H. Essabir, R. Bouhfid, A. el kacem Qaiss, *Structural Health Monitoring of Biocomposites, Fibre-Reinforced Composites and Hybrid Composites*, 277–293 (2019)
53. K. Slámečka, J. Pokluda, P. Ponížil, S. Major, P. Šandera, *Engineering Fracture Mechanics*. **75** (2008), doi:10.1016/j.engfracmech.2007.01.018
54. W. Macek, R. Branco, M. Szala, Z. Marciniak, R. Ulewicz, N. Sczygiol, P. Kardasz, *Materials*. **13**, 3691 (2020)
55. W. Macek, S. Faszynka, A. Deptuła, in *Mechatronics 2017 - Ideas for Industrial Applications* (2019), pp. 290–297
56. W. Macek, M. Szala, M. Kowalski, J. Gargasas, A. Rehmus-Forc, A. Deptuła, *IOP Conference Series: Materials Science and Engineering*. **710**, 012035 (2019)
57. W. Macek, *Engineering Failure Analysis*. **105**, 1154–1171 (2019)
58. W. Macek, *Engineering Failure Analysis*. **99**, 97–107 (2019)
59. W. Macek, D. Rozumek, G. M. Królczyk, *Measurement*. **152**, 107347 (2020)
60. W. Macek, R. Owsiński, J. Trembacz, R. Branco, *Mechanics of Materials* (2020), doi:10.1016/j.mechmat.2020.103410
61. N. Senin, A. Thompson, R. K. Leach, *Measurement Science and Technology* (2017), doi:10.1088/1361-6501/aa7ce2
62. International Organisation of Standardization, ISO 25178. *Geometric Product Specifications (GPS) – Surface texture: areal* (2010)
63. W. Macek, E. Macha, *Solid State Phenomena* (2010), doi:10.4028/www.scientific.net/SSP.164.67
64. W. Macek, E. Macha, *Archive of Mechanical Engineering*. **62** (2015), doi:10.1515/meceng-2015-0006
65. L. Kasprzyczak, E. Macha, Z. Marciniak, *Energy parameter control system of strength machine for material tests under cyclic bending and torsion* (2013), vol. 198
66. Z. Marciniak, D. Rozumek, E. Macha, *International Journal of Fatigue* (2008), doi:10.1016/j.ijfatigue.2007.07.001
67. Z. Marciniak, D. Rozumek, E. Macha, *International Journal of Fatigue* (2014), doi:10.1016/j.ijfatigue.2013.02.021
68. H. Ipakchi, A. M. Rezadoust, M. Esfandeh, M. Rezaei, *Thin-Walled Structures*. **151** (2020), doi:10.1016/j.tws.2020.106724
69. R. Masoudi Nejad, M. Shariati, K. Farhangdoost, *Tribology International*. **94**, 118–125 (2016)
70. W. Kaplonek, K. Nadolny, G. M. Królczyk, The use of focus-variation microscopy for the assessment of active surfaces of a new generation of coated abrasive tools. *Measurement Science Review* (2016), , doi:10.1515/msr-2016-0007
71. L. Newton, N. Senin, C. Gomez, R. Danzl, F. Helmli, L. Blunt, R. Leach, *Additive Manufacturing*. **25**, 365–389 (2019)
72. G. M. Krolczyk, R. W. Maruda, J. B. Krolczyk, P. Nieslony, S. Wojciechowski, S. Legutko, *Measurement: Journal of the International Measurement Confederation*. **121**, 225–239 (2018)